

Experimental and simulation approach of cooling system in 3-phase inverter using extended surface

Agus Mukhlisin^{1,2}, Prisma Megantoro¹, Estiko Rijanto³, I Nyoman Sutantra², Lilik Jamilatul Awal¹,
Yoga Uta Nugraha¹, Indra Sidharta²

¹Electrical Engineering Department, Faculty of Advanced Technology and Multidiscipline, Airlangga University, Surabaya, Indonesia

²Mechanical Engineering Department, Institut Teknologi Sepuluh Nopember, Surabaya, Indonesia

³Research Center for Smart Mechatronics, National Research and Innovation Agency (BRIN), Jakarta Pusat, Indonesia

Article Info

Article history:

Received Apr 19, 2022

Revised Aug 1, 2022

Accepted Aug 17, 2022

Keywords:

3-phase inverter
Cooling system
Extended surface
Heat dissipation
Heat sinks

ABSTRACT

Overheating is a failure mode that significantly affects the reliability of electronic devices. All electronic devices, including a 3-phase inverter driving a traction motor, produce heat dissipation. Heat dissipation needs to be controlled with cooling to prevent overheating. Overheating can be avoided by increasing cooling or reducing heat dissipation. Heat dissipation in the 3-phase inverter is caused by the internal resistance of the metal-oxide-semiconductor field-effect transistor (MOSFET), switching loss, and other factors. Cooling for the 3-phase inverter can use water coolant or air coolant. The cooling system is based on the amount of heat dissipation produced. Cooling of a 3-phase inverter can use air coolant with the addition of an extended surface area in the heat sink. The heat sink uses aluminum material, often called pin fin. There are kinds of aluminum available in the market. We calculated heat generation based on the MOSFET's internal resistance, switching loss, and other factors. We validated the simulation results experimentally using a thermal camera. Thus, we could find an optimal number, dimensions, and aluminum type of fin for the cooling system in the 3-phase inverter.

This is an open access article under the [CC BY-SA](https://creativecommons.org/licenses/by-sa/4.0/) license.



Corresponding Author:

Agus Mukhlisin

Department of Electrical Engineering, Faculty of Advanced Technology and Multidiscipline

Airlangga University

Gedung Kuliah Bersama, Campus C, Mulyorejo, Surabaya 60115, Indonesia

Email: agus.mukhlisin@ftmm.unair.ac.id

1. INTRODUCTION

Electronic component reliability is influenced by a cooling system [1]. Each electronic component will produce heat dissipation, including the 3-phase inverter for a motor controller. Heat dissipation needs to be controlled with a cooling system to prevent overheating. It can also be done by reducing the amount of heat dissipation produced, such as using the right switching strategy [2]–[4], using field-oriented control (FOC) [5], [6], using intelligent control [7]–[11], and the others. The most dominant heat source in the motor controller is losses in the 3-phase inverter. Part of the 3-phase inverter that will produce heat is the metal-oxide-semiconductor field-effect transistor (MOSFET).

One of the MOSFET failure modes is overheating. The heat generated by MOSFETs must be transferred quickly to the cooling media with intelligent cooling using a fan [12], thermoelectric cooling [13], others so that the temperature of the MOSFET does not rise above its ability limit. Heat transfer can occur in several ways, including the following: conduction, convection, and radiation [14]–[16]. This paper will

discuss the MOSFET cooling method using an extended surface (pin fin). The extended surface area of heat transfer improves the thermal efficiency [17], [18].

Computational fluid dynamic (CFD) simulation can be used to obtain a cooling method that suits your needs [19], [20]. This method can help to analyze the cooling method without spending time doing experiments [21]. The numerical method can show the temperature distribution and how much heat must be cooled [22]. If the final design has been obtained, this design can be used as a reference in making a prototype. This work presents optimized heat transfer from MOSFET in a 3-phase inverter by using extended surfaces with some pin fins and dimensions. The calculation of heat loss in the 3-phase inverter is used as the input in the simulation. The simulation result is validated with the experimental results. The validation is carried out based on the temperature distribution and the temperature's value at the same point. If the error tolerance that occurs does not exceed 5%, we consider that an accurate simulation is obtained. Therefore, it can be used to optimize the number of fins and the dimensions of the fins. Our target is that the 3-phase inverter can operate normally at a power of 30 kW.

2. METHOD

First, we performed a heat loss calculation in 3-phase inverter for parameter input in the simulation. Next, the simulation results were validated with the experimental results, where the temperature distribution was obtained using a thermal camera. After the simulation results are validated, it is possible to optimize the heat sink according to the heat loss. As a result, the optimal heat sink configuration is obtained with the controller not overheating.

Heat losses can be seen in the power flow diagram in Figure 1. Based on Figure 1, the 3-phase inverter losses consist of conduction loss pulse-code modulation PCM, switching loss part submission warrant PSW, dead time loss PD, and gate charge loss PG, as given in (1) to (4) [23], [24].

$$P_{CM} = \frac{1}{T_{SW}} \int_0^{T_{SW}} p_{CM}(t) dt = \frac{1}{T_{SW}} \int_0^{T_{SW}} R_{DSon} \cdot i_D^2(t) dt = R_{DSon} \cdot I_{Drms}^2 \tag{1}$$

$$P_{SW} = \frac{1}{2} V_{IN} \cdot I_o \cdot (t_r + t_f) \cdot f_{SW} \tag{2}$$

$$P_D = V_D \cdot I_o \cdot (t_{Dr} + t_{Df}) \cdot f_{sw} \tag{3}$$

$$P_G = (Q_{g-H} + Q_{g-L}) \cdot V_{gs} \cdot f_{sw} \tag{4}$$

The symbol R_{DSon} is the MOSFET drain-source internal resistance (Ω), T_{SW} is switching time (s), i_D is the current flowing in drain (A), and I_{Drms} is the current flowing from source to drain (A). V_{in} and I_o represent the battery voltage (V) and the output current (A). t_r is the rise time of the MOSFET (s), t_f is the fall time of the MOSFET (s), and f_{sw} is the switching frequency (Hz). V_D , t_{Dr} , and t_{Df} denote the low-side MOSFET – diode forward-voltage (Volt), dead-time at rising (s), and dead-time at falling (s). V_{gs} is the gate drive voltage of the MOSFET (V), Q_{g-H} is the high side MOSFET gate electric charge (C), and Q_{g-L} is the low side MOSFET gate electric charge (C). This controller uses the type of MOSFET IRFB4115 with the specifications shown in Figure 2.

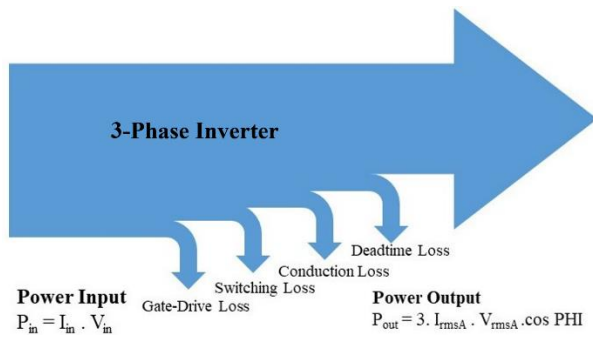
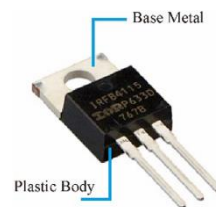


Figure 1. Power flow 3-phase inverter



$R_{DS(on)}$ max	: 11 m Ω
Maximum Temperature	: 175 $^{\circ}$ C
Turn-On Delay ($t_{d(on)}$)	: 18 ns
Rise Time (t_r)	: 73 ns
Turn-off Delay ($t_{d(off)}$)	: 41 ns

Figure 2. MOSFET IRFB4115 specification [25]

This controller has the following target specifications; i) maximum voltage operation 150 VDC, ii) maximum power 30 KW, and iii) using an air-cooling system. We first made a simplified 3D model of the 3-phase inverter for numerical analysis using CFD software, as shown in Figure 3. The heat source on the 3-phase inverter is the MOSFET component. So that heat transfer can be analyzed with thermal resistance as shown in Figure 4.

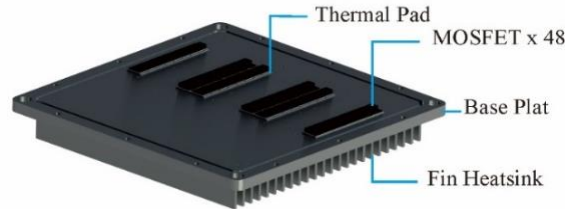


Figure 3. Simplification of 3D model of the 3-phase inverter

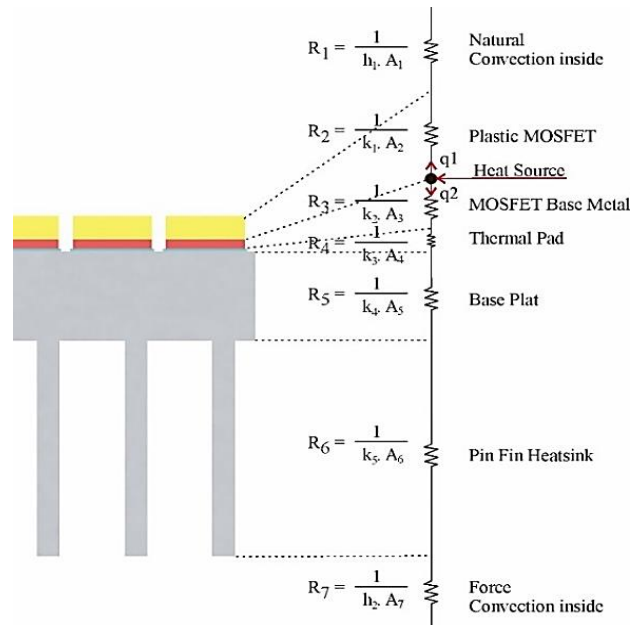


Figure 4. Thermal resistance model controller

The heat source from the MOSFET moves either up to the controller cover or down to the heat sink. The heat transfer downward will be more dominant than upward. The controller cover traps the air contained inside the controller container, so it does not allow air circulation. The heat transmitted downward propagates through the thermal pad.

A thermal pad is a component that serves as an insulator between the base metal of the MOSFET and the heat sink. The use of the thermal pad must have good thermal conductivity as well as a good insulator. The motor controller failure can also be caused by improper thermal pad selection. If the heat generated by the MOSFET is not transferred to the heat sink quickly, the MOSFET will experience overheating, resulting in failure. Similarly, if the thermal pad cannot isolate the metal base of the MOSFET, a short circuit will occur, and the controller will fail. Generally, the thermal pad uses silicone material. The heat transfer then continues to the heat sink fin by conduction. The equation of heat transfer by conduction is given in [14], [16]:

$$q_{conduction} = k \cdot A \cdot \Delta T \tag{5}$$

The type of heatsink material affects the quality of heat transfer: the more significant the heat sink material's thermal conductivity (k), the more remarkable its heat propagation ability. Our heat sink uses 1060 series

aluminum material, often found in the local market. Convection sends the heat transfer into the air around the heat sink fin. The equation of heat transfer by convection is given by (6) to (8) [14], [16]:

$$q_{convection} = h \cdot A \cdot \Delta T \quad (6)$$

$$Nu = \frac{h \cdot L}{k_f} = f(Re_L, Pr) \quad (7)$$

$$Re_L = \frac{\rho \cdot V \cdot L}{\mu} \quad (8)$$

The symbols h and A represent the convection coefficient (W/m²K) and the heat transfer area (m²). L is the length of material (meters), k_f is the thermal conductivity of the fluid (W/mK), and Nu is the Nusselt number. Re and Pr denote Reynold's number and Prandtl's number. ρ is the density of air (kg/m³), V is the velocity of air (m/s), and μ is the friction coefficient.

Convection heat transfer can be optimized by increasing the convection coefficient and cooling area. Increasing the convection coefficient can be done by increasing the speed of air flowing at the fin heat sink, for example, by adding a fan, directing the air with a guide fan so that air can be directed precisely at the heatsink. The cooling area can be enlarged by using variations in dimension and the number of fins on the heatsink. The quality of the simulation results is determined by the dimensions and meshing used. Our meshing uses a curvature-based parameter mesh with total nodes of 615,925, using Jacobian points by 4 points. Table 1 lists material types used in the motor controller cooling simulation. Figure 5 shows the meshing model.

Table 1. Material types for cooling simulation

Component	Materials	Thermal conductivity (W/mK)
Fin heat sink	Aluminum 1060	200
Base plat	Aluminum 1060	200
Thermal pad	Silicone	3.2
MOSFET plastic body	Plastic Silicone	124
MOSFET base metal	Aluminum 5052	137

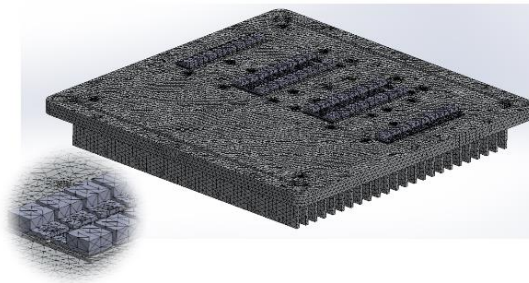


Figure 5. Meshing model

Connection contact set using bounded type. The contact that needs to be defined is between MOSFET with the thermal pad and the thermal pad with the heat sink. This step ensures that the connections between different materials are perfectly connected. We conducted numerical simulation using CFD with the following conditions:

- Surrounding temperature: 28 °C
- Controlled variable: Convection coefficient (h)
- The source of the heat loss: the MOSFET

First, we calculated heat loss when the motor controller is under a 1.5 kW load as show in Table 2. Afterward, the simulation can be run, and temperature distribution can be obtained. Simulation results will be validated using experimental results. Experiments with a maximum load of 30 kW continuously (30 minutes) cannot be done because the dynamometer will overheat. So, the experiment was carried out with a continues load of 1.5 kW. Furthermore, the results of these experiments can be used to validate the simulation results. The validated simulation results can then be used to test the maximum loading, so that the temperature

distribution is obtained when the maximum loading to obtain the temperature distribution under the maximum loading. This simulation can also be used to optimize the fin on the heat sink so that cooling is obtained as needed with minimum fin dimensions.

Figure 6 shows the experimental setup with (a) schema of experiment and (b) installed equipment in this paper. It is equipped with an eddy current dynamometer paired with a 30 KW motor. The temperature sensor uses a 10K thermistor recorded in a datalogger (USB to CAN Datalogger). An oscilloscope with four channels is used to measure voltage and current, both input and output. A thermal camera is used to obtain the temperature distribution.

Table 2. Calculated heat loss in the motor controller under 1.5 kW load

Type Heat Loss	Parameter	Value
Conduction Loss	$R_{DS(on)} = 11 \text{ m}\Omega$; $I_D = 8.15 \text{ A}$; $V_{in} = 80.34 \text{ V}$;	0.617 W
Switching Loss	$t_r = 73 \text{ ns}$; $t_f = 39 \text{ ns}$; $f_{SW} = 20 \text{ kHz}$;	0.733 W
Deadtime Loss	$t_{d(on)} = 18 \text{ ns}$; $t_{d(off)} = 41 \text{ ns}$; $V_{gs} = 23 \text{ V}$; $Q_g = 120 \text{ nC}$.	0.772 W
Gate Charge Loss		0.055 W
Total Heat Loss		2.177 W

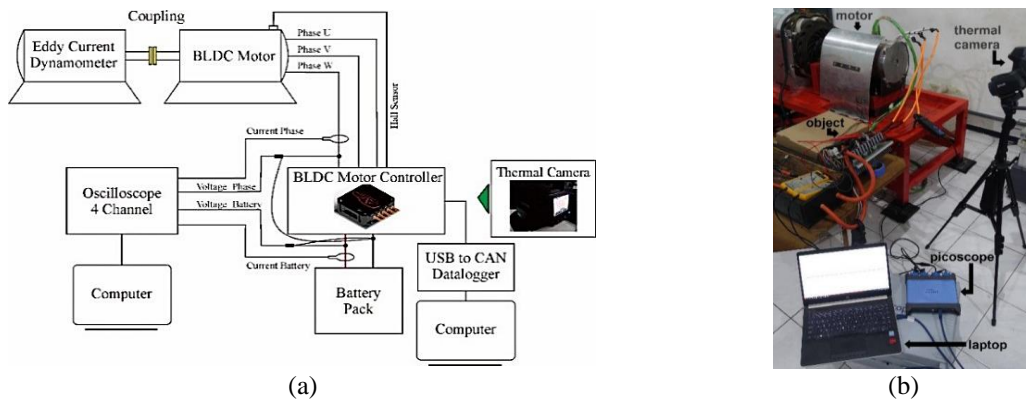


Figure 6. Experiment setup (a) schema and (b) equipment

3. RESULTS AND DISCUSSION

3.1. Simulation validation through experiment

The load was kept constant at 1.5 kW with a motor speed of 950 rpm and variations in wind speed. We changed wind speed by controlling a fan power to obtain speed 1, speed 2, and speed 3. CAN to USB datalogger was used to obtain data, among others: temperature of heat sink, phase current, battery current, battery voltage, and the motor speed. One-time data collection took 35 minutes or until the heat sink temperature got steady. The result of the experiment is shown in Figure 7.

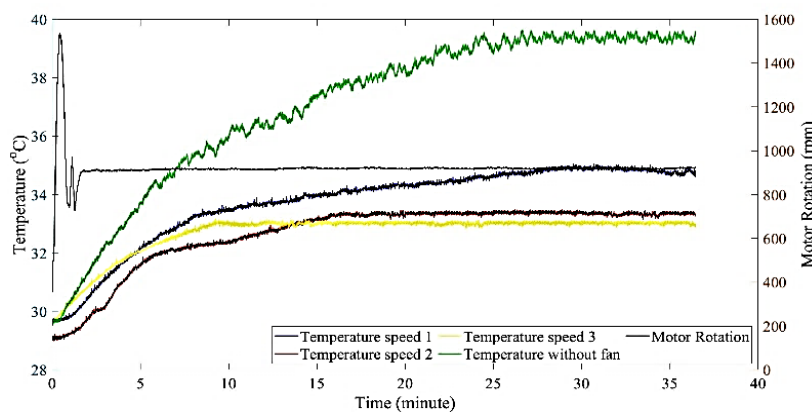


Figure 7. Motor speed and heat sink temperature

The heat sink temperatures in Figure 7 were measured using a thermistor sensor. Yellow, red, blue, and green line curves are the heat sink temperatures with variations in wind speed 1, speed 2, speed 3, and natural convection. Each line's steady-state temperature is yellow at 33.37 °C, red at 33.96 °C, blue at 34.92 °C, and green at 39.72 °C. The greater wind speed yields a lower temperature of the heat sink. This is in accordance with (6), (7), and (8). The trend line that occurs tends to be steady at a specific time. This indicates that the cooling is sufficient so that overheating will not occur. The temperature distribution can be captured in this steady state with a thermal camera.

Figures 8 and 9 show the temperature distribution results obtained from the simulation and experiment. Figure 8 shows the temperature distribution using $h=40 \text{ W/m}^2\text{K}$, both experimentally and in simulation results. Figure 8(a) shows the simulation results where the thermistor sensor laying point shows a temperature of 33.1 °C. While Figure 8(b) is a photo taken by the thermal camera where the location of the thermistor shows the value of 33.3 °C. These results indicate that the simulation results have a 0.6% error. The temperature distribution in general also has similarities. Under continuous loading of 1.5 kW, the highest temperature occurs in the DC-DC converter, yielding 37 °C.

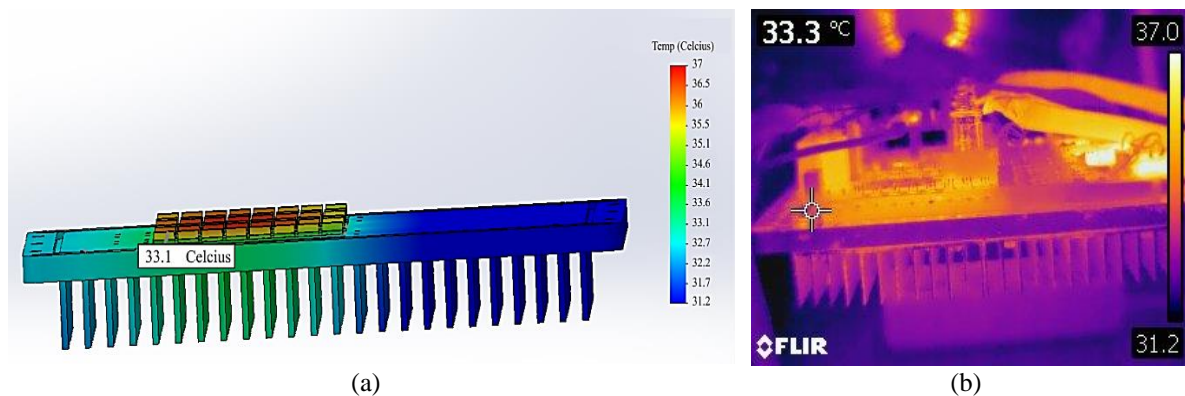


Figure 8. Temperature distribution with $h=40 \text{ W/m}^2\text{K}$ (a) simulation result and (b) experiment result

Figure 9 shows the temperature distribution using $h=33 \text{ W/m}^2\text{K}$ for both experimental and simulation results. Figure 9 (a) shows the simulation results where the thermistor sensor laying point shows a temperature of 34.3 °C. In comparison, Figure 9 (b) is a photo taken by the thermal camera where the location of the thermistor shows the value of 34.9 °C. The result indicates that the simulation results have a 1.75% error. Based on the results shown in Figures 8 and 9, the simulation results can be accepted with an error tolerance of $\pm 1.75\%$. Furthermore, the simulation method can be used to evaluate the maximum loading of the 3-phase inverter, i.e., with a load of 30 kW. Table 3 summarizes the data obtained from the simulation and experimental results.

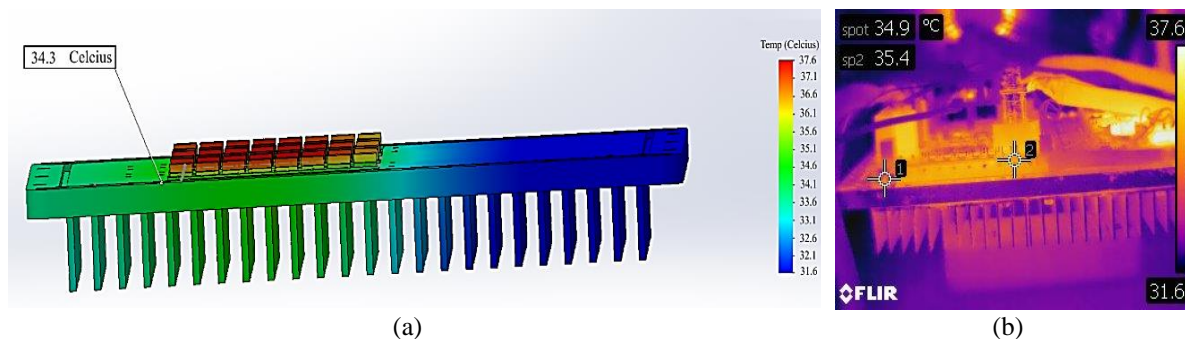


Figure 9. Temperature distribution with $h=33 \text{ W/m}^2\text{K}$ (a) simulation result and (b) experiment result

Table 3. Comparison of simulation with experiment results

Coefficient of Convection	Experiment	Simulation	Percentage of Error
$h=33 \text{ W/m}^2\text{K}$	34.9 °C	34.3 °C	1.75 %
$h=40 \text{ W/m}^2\text{K}$	33.1 °C	33.3 °C	0.6 %

3.2. Optimization of the heat sink under maximum load

We calculated heat loss produced by each MOSFET when the 3-phase inverter operates under the maximum load 30 kW. Table 4 shows the parameter values and the heat loss values. Since we have 48 MOSFETs, the total heat loss is 1,048.27 Watts. We used this heat loss value as the input to our CFC model and conducted a numerical simulation. Figure 10 shows the temperature distribution of the heat sink under a maximum load of 30 kW. The maximum temperature is 98.9 °C, so the controller does not overheat. The temperature where the MOSFET is situated shows a value of 38.5 °C. Since the temperature is significantly lower than the critical temperature of the MOSFET, the heat sink fin is not required in this area.

Table 4. Heat loss of each MOSFET in the motor controller under 30 kW Load

Type Heat Loss	Parameter	Value
Conduction Loss	$R_{DS(on)}=11 \text{ m}\Omega$; $I_D=65.16 \text{ A}$; $V_{in}=80.34 \text{ V}$;	14.491 W
Switching Loss	$t_r=73 \text{ ns}$; $t_f=39 \text{ ns}$; $f_{SW}=20\text{kHz}$;	3.551 W
Deadtime Loss	$t_{d(on)}=18 \text{ ns}$; $t_{d(off)}=41\text{ns}$; $V_{gs}=23\text{V}$; $Q_g=120 \text{ nC}$.	3.742 W
Gate Charge Loss		0.055 W
Total Heat Loss		21.839 W

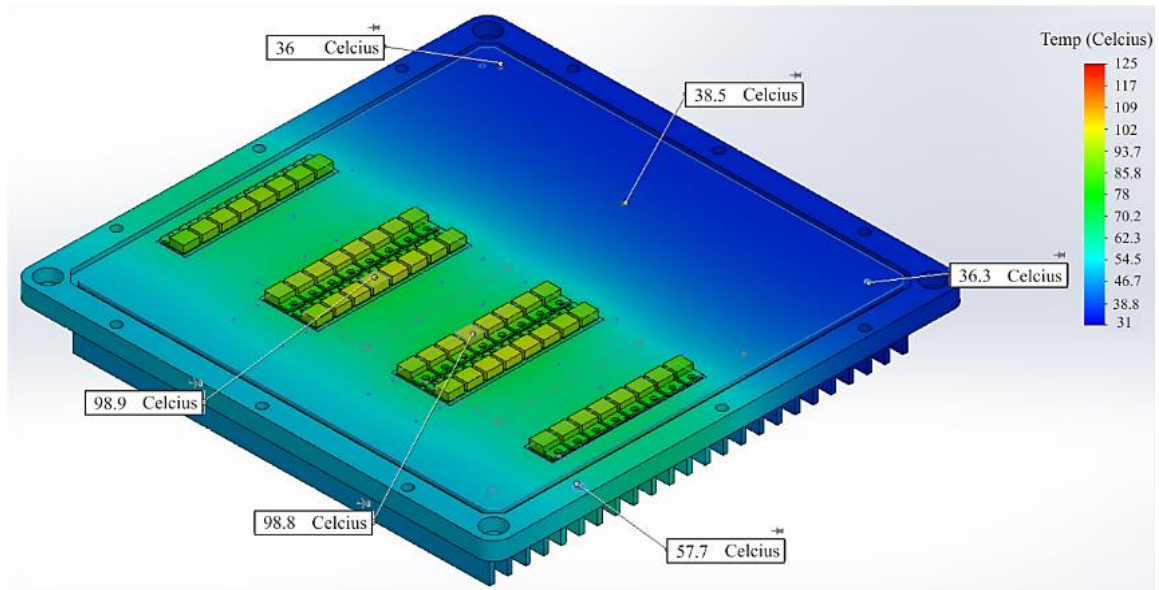


Figure 10. Simulation result under maximum load 30 kW

Furthermore, we optimized the number and length of the heat sink fins with maximum thermal load and $h=60 \text{ W/m}^2\text{K}$. The original length of each heat sink fin is 20 mm. Figure 11 shows the simulation results. Figure 11(a) shows the temperature distribution using 15 pieces of heat sink fins. The highest temperature of the MOSFET is 103 °C. The temperature is lower than the critical operation temperature of the MOSFET, which is 125 °C. Figure 11(b) shows the temperature distribution using 12 pieces of heat sink fins. The highest temperature of the MOSFET is 107 °C. The result indicates that reducing of fin number to 12 pieces yielding maximum temperature that is lower than the critical temperature of the MOSFET. Further optimization is carried out by reducing the fin length to 12 mm and yielding the temperature distribution shown in Figure 11(c). The maximum temperature of the MOSFET in this condition is 117 °C, which is lower than the critical temperature of MOSFET. However, there is an increase in temperature compared to the result of 12 pieces 20 mm fin. Therefore, the controller under a maximum load of 30 kW is optimally cooled using the configuration of 12 pieces of fins with 12 mm length, following Figure 11(c).

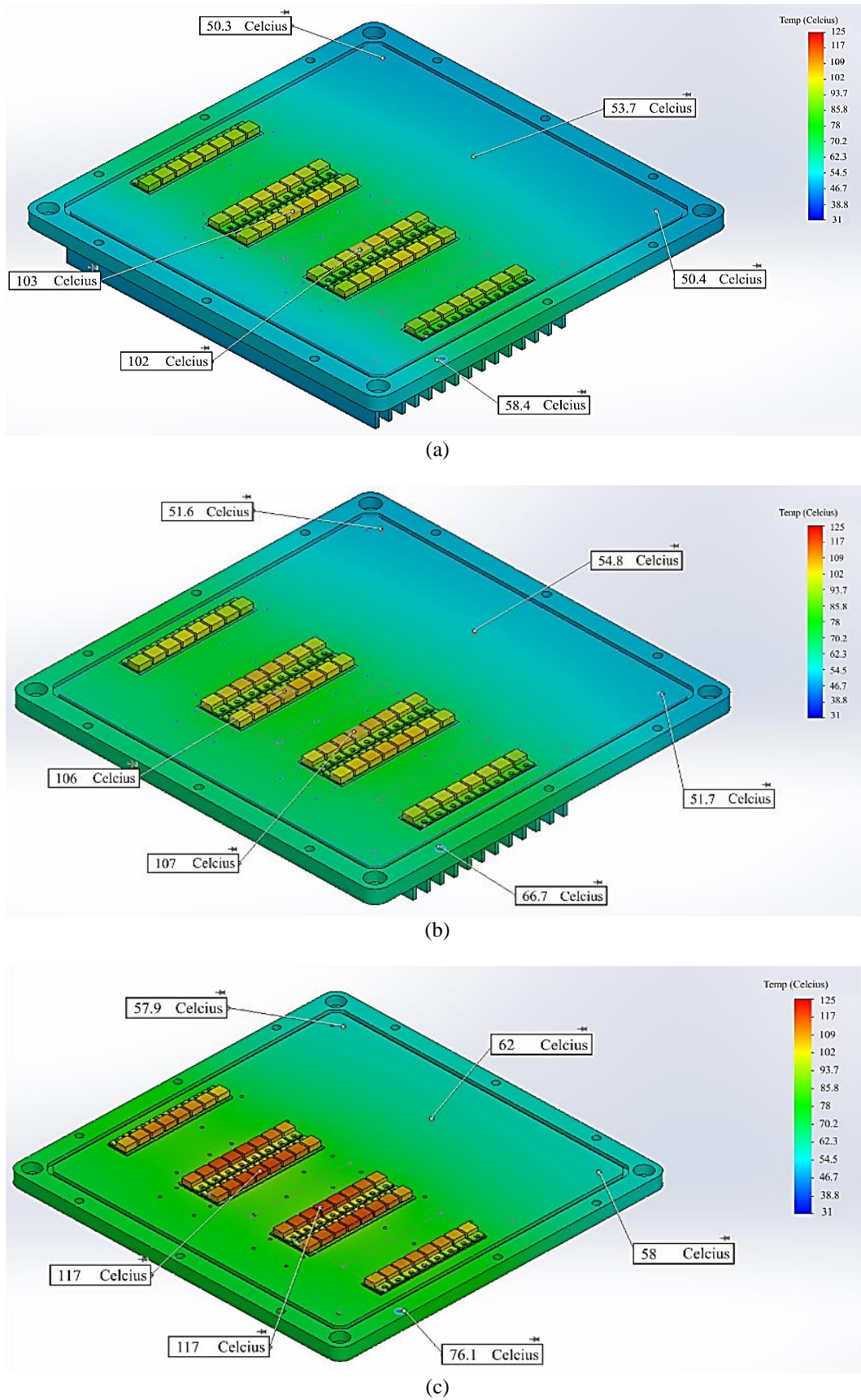


Figure 11. Optimized heat sink in the number and length of the fins: (a) 15 pieces of 20 mm long, (b) 12 pieces of 20 mm long, and (c) 12 pieces of 12 mm long

4. CONCLUSION

Thermal analysis of the controller cooling system was carried out using modeling and simulation. The simulation was validated experimentally with an error of $\pm 1.75\%$. Furthermore, the simulation method can be used to optimize the cooling design for a maximum loading of 30 kW. The results indicate that the controller does not experience overheating, as demonstrated by the MOSFET temperature. Further optimization, through simulation was carried out in order to reduce the size and the number of the fin. The simulation result of the optimized heat sink suggests that the maximum temperature of the MOSFET is lower than its critical temperature. Hence, the controller did not experience overheating.

ACKNOWLEDGEMENTS

Author thanks to Faculty of Advanced Technology and Multidiscipline, Airlangga University and Lembaga Pengelola Dana Pendidikan (LPDP) in most cases, sponsor and financial support acknowledgments. This program support Sustainable Development Goals (SDGs) for affordable and clean energy also goal 9 for Industry, Innovation and Infrastructure.

REFERENCES

- [1] E. Laloya, Ó. Lucía, H. Sarmago and J. M. Burdío, "Heat management in power converters: from state of the art to future ultrahigh efficiency systems," *IEEE Transactions on Power Electronics*, vol. 31, no. 11, pp. 7896-7908, 2016, doi: 10.1109/TPEL.2015.2513433.
- [2] N. A. Ramli, A. Jidin, Z. Rasin, and T. Sutikno, "Reduction of total harmonic distortion of three-phase inverter using alternate switching strategy," *International Journal of Power Electronics and Drive Systems*, vol. 12, no. 3, pp. 1598-1608, 2021, doi: 10.11591/ijpeds.v12.i3.pp1598-1608.
- [3] D. Christen and J. Biela, "Analytical switching loss modeling based on datasheet parameters for mosfets in a half-bridge," *IEEE Transactions on Power Electronics*, vol. 34, no. 4, pp. 3700-3710, 2019, doi: 10.1109/TPEL.2018.2851068.
- [4] A. V. Sant and K. R. Rajagopal, "PM synchronous motor speed control using hybrid fuzzy-pi with novel switching functions," *IEEE Transactions on Magnetics*, vol. 45, no. 10, pp. 4672-4675, 2009, doi: 10.1109/TMAG.2009.2022191.
- [5] V. T. Ha, N. T. Lam, V. T. Ha, and V. Q. Vinh, "Advanced control structures for induction motors with ideal current loop response using field oriented control," *International Journal of Power Electronics and Drive System*, vol. 10, no. 4, pp. 1758-1771, 2019, doi: 10.11591/ijpeds.v10.i4.pp1758-1771.
- [6] M. Hasoun, A. el Afia, M. Khafallah, and K. Benkirane, "Field oriented control based on a 24-sector vector space decomposition for dual three-phase pmsm applied on electric ship propulsion," *International Journal of Power Electronics and Drive Systems*, vol. 11, no. 3, pp. 1175-1187, 2020, doi: 10.11591/ijpeds.v11.i3.pp1175-1187.
- [7] D. Brahim, B. Mokhtar, and L. Salah, "Improvement of adaptive fuzzy control to adjust speed for a doubly fed induction motor drive (DFIM)," *International Journal of Power Electronics and Drive Systems*, vol. 11, no. 1, pp. 496-504, 2020, doi: 10.11591/ijpeds.v11.i1.pp496-504.
- [8] E. Sabouni, B. Merah, and I. K. Bousserhane, "Adaptive backstepping controller design based on neural network for pmsm speed control," *International Journal of Power Electronics and Drive Systems*, vol. 12, no. 3, pp. 1940-1952, 2021, doi: 10.11591/ijpeds.v12.i3.pp1940-1952.
- [9] A. Nait Seghir, T. Henni and M. Azira, "Fuzzy and adaptive fuzzy PI controller-based Vector control for permanent magnet synchronous motor," *10th Ieee International Conference On Networking, Sensing And Control (ICNSC)*, 2013, pp. 491-496, doi: 10.1109/ICNSC.2013.6548788.
- [10] Jae Sung Yu, Sun Mo Hwang and Chung-Yuen Won, "Performances of fuzzy-logic-based vector control for permanent magnet synchronous motor used in elevator drive system," *30th Annual Conference of IEEE Industrial Electronics Society, IECON*, 2004, vol. 3, pp. 2679-2683, doi: 10.1109/IECON.2004.1432229.
- [11] N. J. Patil, R. H. Chile and L. Waghmare, "Fuzzy adaptive controllers for speed control of PMSM drive," *International Journal of Computer Applications*, vol. 1, no. 11, pp. 975-8887, 2010, doi: 10.5120/233-387.
- [12] A. Deep, J. Singh, Y. Narayan, S. Chatterji and L. Mathew, "Intelligent cooling system for three level inverter," *Communication, Control and Intelligent Systems (CCIS)*, pp. 286-289, 2015, doi: 10.1109/CCIntels.2015.7437925.
- [13] U. Sanver, E. Yavuz and C. Eypuglu, "An electronic control unit for thermoelectric cooling," *IEEE Conference of Russian Young Researchers in Electrical and Electronic Engineering (EIConRus)*, 2019, pp. 141-145, doi: 10.1109/EIConRus.2019.8656871.
- [14] F. P. Incropera, D. Witt, T. L. Bergman, and A. S. Lavine, *Fundamentals of heat and mass transfer*, Sixth Edition. New Jersey: John Wiley & Sons, 2006.
- [15] A. Blinov, D. Vinnikov, and T. Lehtla, "Cooling methods for high-power electronic systems," *Scientific Journal of Riga Technical University, Power and Electrical Engineering*, vol. 29, no. 1, pp. 79-86, 2011, doi: 10.2478/v10144-011-0014-x.
- [16] Y. A. Çengel, *Heat Transfer: A Practical Approach*, New York, NY, USA: McGraw-Hill, 2003.
- [17] S. S. Kang, "Advanced cooling for power electronics," *7th International Conference on Integrated Power Electronics Systems (CIPS)*, 2012, pp. 1-8.
- [18] A. Driss, S. Maalej and M. C. Zaghdoudi, "Thermal modeling of the cooling of a power MOSFET by heat pipes," *International Conference on Engineering & MIS (ICEMIS)*, 2017, pp. 1-6, doi: 10.1109/ICEMIS.2017.8273067.
- [19] U. SanAndres, G. Almandoz, J. Poza and G. Ugalde, "Design of cooling systems using computational fluid dynamics and analytical thermal models," *IEEE Transactions on Industrial Electronics*, vol. 61, no. 8, pp. 4383-4391, Aug. 2014, doi: 10.1109/TIE.2013.2286081.
- [20] Y. Bulut and K. Pandya, "Thermal modeling for power MOSFETs in DC/DC applications," *5th International Conference on Thermal and Mechanical Simulation and Experiments in Microelectronics and Microsystems*, 2004, pp. 429-433, doi: 10.1109/ESIME.2004.1304074.
- [21] O. Spuiber, M. M. De Souza, E. M. S. Narayanan and S. Krishnan, "Analyses of a COOL-MOSFET," *CAS '99 Proceedings. 1999 International Semiconductor Conference (Cat. No.99TH8389)*, 1999, pp. 131-134 vol. 1, doi: 10.1109/SMICND.1999.810446.

- [22] M. Langer, Z. Lisik and J. Podgorski, "Numerical simulation of cool MOS transistor," *Experience of Designing and Applications of CAD Systems in Microelectronics. Proceedings of the VI-th International Conference, CADSM*, 2001, pp. 303-304, doi: 10.1109/CADSM.2001.975849.
- [23] G. Dusan, M. Purschel, and A. Kiep, "MOSFET power losses calculation using the data-sheet parameters," *Infineon application note*, pp. 1-23, 2006.
- [24] ROHM Semiconductor, "Application Note: Calculation of Power Loss (Synchronous)," 2016. [Online]. Available: http://rohms.rohm.com/en/products/databook/applinote/ic/power/switching_regulator/power_loss_appli-e.pdf.
- [25] International IOR Rectifier, "IRFB4115PbF HEXFET Power MOSFET Datasheet," 2014. [Online]. Available: <https://www.infineon.com/dgdl/irfb4115pbf.pdf?fileId=5546d462533600a401535615ba6a1e0f>.

BIOGRAPHIES OF AUTHORS



Agus Mukhlisin    is a lecturer in Electrical Engineering Department at Faculty of Advanced Technology and Multidiscipline, Airlangga University, Surabaya, Indonesia. He received a Bachelor's degree and Master's degree from Institute Technology of Sepuluh November, Surabaya, Indonesia in 2015 and 2017. He is currently pursuing Doctoral Program in Institute Technology of Sepuluh November, Surabaya, Indonesia. His Dissertation Topic was about Intelligent Vector Control in Motor Controller. His research interests include System and Control of Electric Vehicle, Battery Management System, Charging Station, and Dynamic System Simulation. He can be contacted at email: agus.mukhlisin@ftmm.unair.ac.id.



Prisma Megantoro    is a lecturer in Electrical & Electronic Engineering Department, Faculty of Advanced Technology and Multidiscipline, Airlangga University, Surabaya, Indonesia. He received the bachelor degree and master degree from Universitas Gadjah Mada, Yogyakarta, Indonesia in 2014 and 2018. His current research is focused on solar photovoltaic technology, embedded system, and internet of things. He can be contacted at email: prisma.megantoro@ftmm.unair.ac.id.



Estiko Rijanto    has worked for Research Center for Smart Mechatronics - the National Research and Innovation Agency (BRIN) - Indonesia since 2021. From 2002 to 2021, he worked at Research Center for Electrical Power and Mechatronics, Indonesian Institute of Sciences (LIPI). In 1987 he enrolled at Institut Teknologi Bandung (ITB). He completed his B.Eng. degree at Tokyo University of Agriculture and Technology (TUAT), Tokyo - Japan, in 1993. He received M. Eng. and Dr. Eng. degrees from the same university in 1995 and 1998. In 2000, he completed his book on "Robust Control: Theory for Application" during his post-doctoral program at TUAT-VBL. In 2013, he was inaugurated as the Research Professor on Applied Control Systems by LIPI after presenting his book "Integration of control and information systems for industrial competitiveness,". His research interests include control systems and their applications for mechatronics, electric vehicles, power generations, renewable energies, and battery management systems. He can be contacted at email: esti003@brin.go.id.



I Nyoman Sutantra    is a lecturer in Mechanical Engineering Department, Institut Teknologi Sepuluh November, Surabaya, Indonesia. He received a Bachelor's degree from Institute Technology of Sepuluh November, Surabaya, Indonesia. He received a Master and Doctoral degree from The University of Wisconsin – Madison in mechanical department. He was inaugurated the Professor on mechanical engineering. His research interests include automotive technology, electric vehicles, hybrid vehicle and steering control. He can be contacted at email: tantra@me.its.ac.id.



Lilik Jamilatul Awalina    is a lecturer in Electrical & Electronic Engineering Department, Faculty of Advanced Technology and Multidiscipline, Airlangga University, Surabaya, Indonesia. She received the bachelor degree from electrical engineering, Widya Gama Malang, Indonesia in 1977. She received the master degree from Institute Technology of Sepuluh November, Surabaya, Indonesia in 2004. Finally, she gets the doctoral degree from University of Malaya, Malaysia in 2014. Her current research is focused on fault localization, smart grid technology, transmission and distribution network, load shedding, coordination protection and optimization. She can be contacted at email: lilik.j.a@ftmm.unair.ac.id.



Yoga Uta Nugraha    is as a lecturer at Electrical Engineering program in the Faculty of Advanced Technology and Multidiscipline, Universitas Airlangga, Surabaya, Indonesia. He was born in Sukoharjo, Central of Java. He is a Doctoral candidate in Electrical Engineering Department of Sepuluh Nopember Institute of Technology Surabaya. He has a Bachelor (2015) and Master (2020) of Electrical Engineering from Sepuluh Nopember Institute of Technology Surabaya. His current research is focused on integration on Electric Vehicle, electric machine, permanent magnet motor, new and renewable energy. He can be contacted at email: yoga.uta.n@ftmm.unair.ac.id.



Indra Sidharta    is a lecturer in Mechanical Engineering Department, Institut Teknologi Sepuluh November, Surabaya, Indonesia. He received a Bachelor's degree from Institute Technology of Sepuluh November, Surabaya, Indonesia in 2004. He received a Master degree from Hamburg University of Technology in field Materials Science, 2010. His current research is focused on metal matrix composite, metallurgy, materials of battery. He can be contacted at email: indra.sidharta@gmail.com.